DALTON
FULL PAPER

Structural, spectroscopic and electrochemical studies of nickel(II) "sandwich" complexes with ligands featuring tethered 1,4,7-triazacyclononane macrocycles †

Bim Graham,[a] Leone Spiccia,*[a] Alan M. Bond,[a] Milton T. W. Hearn[b] and Christopher M. Kepert[a]

[a] *School of Chemistry, PO Box 23, Monash University, 3800, Victoria, Australia. E-mail: leone.spiccia@sci.monash.edu.au*
[b] *Department of Biochemistry and Molecular Biology, PO Box 130, Monash University, 3800, Victoria, Australia*

Received 23rd February 2001, Accepted 22nd May 2001
First published as an Advance Article on the web 19th July 2001

A structural and electrochemical study of the nickel(II) complexes, $[Ni(tacn)_2](ClO_4)_2$ (**1**), $[NiL^{eth}](ClO_4)_2$ (**2**), $[NiL^{ox}](ClO_4)_2 \cdot H_2O$ (**3**), $[Ni_2L^{dur}](ClO_4)_4 \cdot 2H_2O$ (**4**), $[Ni_3L^{dur}(H_2O)_3](ClO_4)_6 \cdot 9H_2O$ (**5**) and $[Ni_2L^{isomes}(H_2O)_3](ClO_4)_4 \cdot 7H_2O$ (**6**) [tacn = 1,4,7-triazacyclononane, L^{eth} = 1,2-bis(1,4,7-triazacyclonon-1-yl)ethane, L^{ox} = 1,2-bis(1,4,7-triazacyclonon-1-ylmethyl)benzene, L^{dur} = 1,2,4,5-tetrakis(1,4,7-triazacyclonon-1-ylmethyl)benzene, L^{isomes} = 1,2,3-tris(1,4,7-triazacyclonon-1-ylmethyl)benzene] is reported. Single-crystal X-ray crystallography has established that **2** and **6** feature nickel(II) centres in a distorted octahedral geometry, which are sandwiched between pairs of tacn rings. In **6**, a second nickel(II) centre coordinates the third tacn ring of L^{isomes} and three water molecules complete the distorted octahedral coordination sphere. For the sandwiched Ni(II) centres, steric contraints introduced by the ethane and *ortho*-oriented tacn rings in L^{isomes} cause significant distortions to the Ni(II) coordination spheres. Cyclic, square-wave and near steady-state voltammetric studies on **1**–**6** indicate that the sandwiched nickel(II) centres may be reversibly oxidised to the nickel(III) state, with the potential for the nickel(II)/(III) couple showing a dependence on the nature of the tether linking the sandwiching tacn rings. Complex **4** undergoes oxidation in two overlapping one-electron processes [*i.e.*, Ni(II)Ni(II) → Ni(III)Ni(II) → Ni(III)Ni(III)], indicating that the two nickel centres within the complex behave in an essentially independent fashion.

Introduction

The metal-complexing properties of the small tridentate macrocycle, 1,4,7-triazacyclononane (tacn), have been extensively studied since its preparation was first detailed in 1972.[1] When reacted with a variety of divalent and trivalent transition metal ions in a 2 : 1 molar ratio, tacn readily forms "sandwich-type" complexes, $[M(tacn)_2]^{n+}$ ($M^{n+} = Cr^{3+}$, Mn^{2+}, Fe^{2+}, Fe^{3+}, Co^{2+}, Co^{3+}, Ni^{2+}, Ni^{3+}), featuring metal centres with octahedral N_6 donor sets.[2,3] A number of groups have reported that various bis(tacn) ligands, composed of pairs of covalently linked tacn macrocycles, can form similar structures, provided the linker group between the sandwiching macrocycles is sufficiently flexible. The first examples were reported by Takamoto *et al.*[4] and Wieghardt *et al.*[5] who described a series of mononuclear complexes of the ethane-bridged bis(tacn) ligand [L^{eth} = 1,2-bis(1,4,7-triazacyclonon-1-yl)ethane; M = Cu^{2+}, $Ni^{2+/3+}$, Mn^{2+}, Zn^{2+}, Fe^{3+}, Co^{3+}, Cr^{3+}] and the propane-bridged bis(tacn) ligand, [L^{prop} = 1,3-*bis*(1,4,7-triazacyclonon-1-yl)propane; M = Co^{3+}]. Zompa and co-workers[6–8] later detailed an in-depth structural and equilibrium study of the copper(II) complexation behaviour of a series of bis(tacn) ligands in which alkyl chains of 2–8 carbons link the tacn rings. It was concluded that L^{eth} forms only the monomeric $[CuL]^{2+}$ complex in dilute aqueous solution whilst the other ligands are capable of forming both $[CuL]^{2+}$ and $[Cu_2L]^{2+}$ complexes, with the stability of the $[CuL]^{2+}$ species decreasing with increasing chain length. The X-ray structures of $[CuL^{eth}]^{2+}$ and $[CuL^{prop}]^{2+}$ confirmed the formation of intramolecular sandwich-type structures, whilst the other $[CuL]^{2+}$ complexes were proposed to be dimeric or oligomeric. For alkyl bridges comprising of ≥4 carbons, intermolecular sandwich structures of the form $[Cu_2L_2]^{4+}$ have been postulated.[6–8] We have recently reported further examples of Ni(II) and Cu(II) complexes of poly(tacn) derivatives.[9,10] The Ni(II) series includes $[NiL^{ox}](ClO_4)_2 \cdot H_2O$ (**3**), $[Ni_2L^{dur}](ClO_4)_4 \cdot 2H_2O$ (**4**) and $[Ni_3L^{dur}(H_2O)_3](ClO_4)_6 \cdot 9H_2O$ (**5**) [L^{ox} = 1,2-bis(1,4,7-triazacyclonon-1-ylmethyl)benzene, L^{dur} = 1,2,4,5-tetrakis(1,4,7-triazacyclonon-1-ylmethyl)benzene].[9,10] At least one Ni centre in these complexes is sandwiched between pairs of tacn macrocycles attached to *ortho* positions of an aromatic spacer group. Detailed equilibrium studies on the series of xylyl-bridged ligands, L^{ox}, L^{mx} and L^{px}, reported by Zompa and co-workers,[8] confirmed that the stability of the sandwich structures decreases in the order $L^{ox} > L^{mx} > L^{px}$.

In this paper, we report the synthesis of a further poly(tacn) ligand, 1,2,3-tris(1,4,7-triazacyclonon-1-ylmethyl)benzene (L^{isomes}), featuring three tacn rings linked by a 1,2,3-trimethylbenzene unit. It was anticipated that this ligand might also be capable of forming complexes incorporating a sandwiched metal centre by virtue of its *ortho* oriented tacn rings. These expectations were confirmed through the isolation of the binuclear complex, $[Ni_2L^{isomes}(H_2O)_3](ClO_4)_4 \cdot 7H_2O$ (**6**). The crystal structure of **6** is presented together with that of the previously reported $[NiL^{eth}](ClO_4)_2$ (**2**). The results of a detailed electrochemical study on the series of nickel(II) sandwich complexes **1**–**6**, shown in Fig. 1, are described. These show that the sandwiched nickel(II) centres can be reversibly oxidised to

† Electronic supplementary information (ESI) available: representative cyclic voltammograms for the mononuclear complex **2** and binuclear complex **4**. See http://www.rsc.org/suppdata/dt/b1/b101766g/

 DOI: 10.1039/b101766g

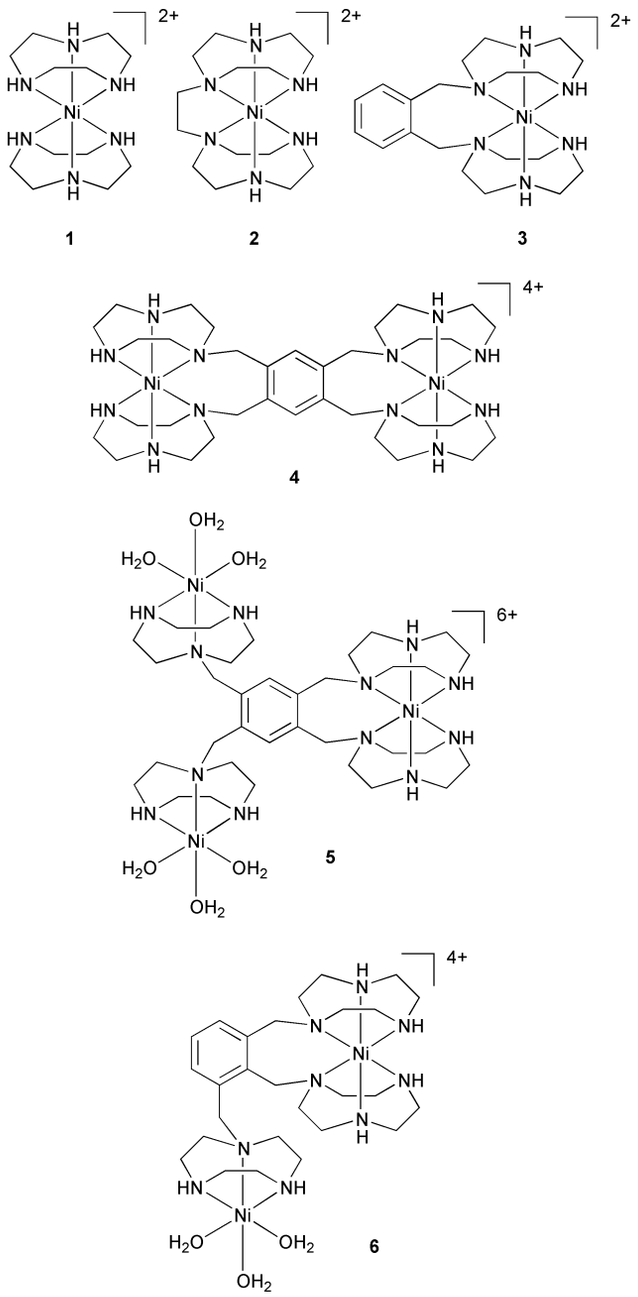

Fig. 1 Nickel(II) complexes featuring sandwiched Ni(II) centres.

the nickel(III) state. The trends in the redox potentials of the nickel(II)/(III) couples are discussed in terms of the solid-state structures of the compounds.

Results and discussion

Syntheses

The synthesis of L^{isomes} was adapted from the method described recently for the related mesitylene-bridged trimacrocycle, 1,3,5-tris(1,4,7-triazacyclonon-1-ylmethyl)benzene.[11] This involved reaction of 3 molar equiv. of tacn orthoamide (1,4,7-triazatricyclo[5.2.1.$0^{4,10}$]decane) with 1,2,3-tri(bromomethyl)benzene, followed by base hydrolytic work-up to yield the crude ligand as a white solid (Scheme 1). Although further purification of the ligand by recrystallisation from various solvents and solvent mixtures was unsuccessful, both the ^{1}H and ^{13}C NMR spectra confirmed the generation of the ligand. The crude L^{isomes} ligand was treated with an excess of Ni^{2+} ions to yield a binuclear complex which, following cation-exchange chromatography (CEC), could be crystallised as the perchlorate salt,

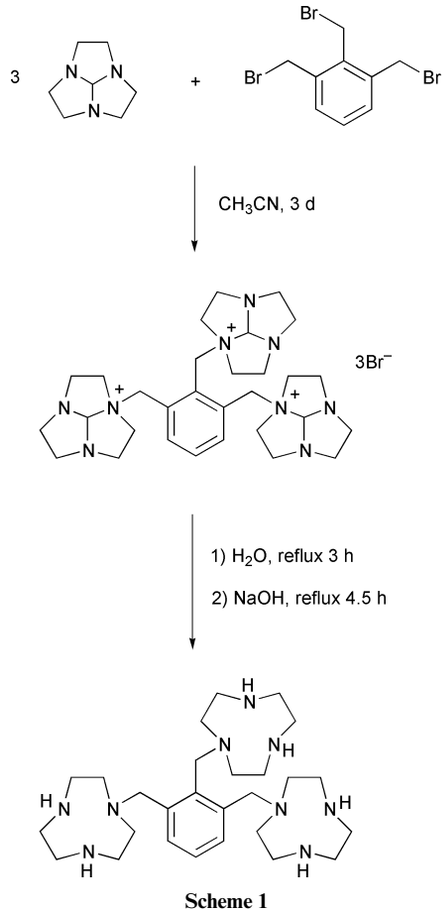

Scheme 1

$[Ni_2L^{isomes}(H_2O)_3](ClO_4)_4\cdot 7H_2O$ (**6**). A small amount of the trinuclear complex, $[Ni_3L^{isomes}(H_2O)_9]^{6+}$, was also formed in the reaction but attempts to isolate this complex as a crystalline salt have thus far proved unsuccessful.

The coordination behaviour of L^{isomes} towards Ni^{2+} ions is reminiscent to that of the L^{ox} and L^{dur} ligands,[9,10] which also feature sets of tacn rings attached to the *ortho* positions of an aromatic spacer. These either coordinate to different Ni^{II} centres or sandwich a single Ni^{II} centre forming the complexes: $[NiL^{ox}](ClO_4)_2\cdot H_2O$ (**3**) and $[Ni_2L^{ox}(H_2O)_6](ClO_4)_4\cdot 4H_2O$ from L^{ox}; and $[Ni_2L^{dur}](ClO_4)_4\cdot 2H_2O$ (**4**), $[Ni_3L^{dur}(H_2O)_3](ClO_4)_6\cdot 9H_2O$ (**5**) and $[Ni_4L^{dur}(H_2O)_{12}](ClO_4)_8\cdot 9H_2O$ from L^{dur}.

The preparations of the nickel(II) sandwich complexes, $[Ni(tacn)_2](ClO_4)_2$ (**1**)[12] and $[NiL^{eth}](ClO_4)_2$ (**2**),[5] have been described previously. We found that **2** forms even under conditions of excess metal ion, an observation which can be ascribed to the fact that a stable five-membered chelate ring, incorporating the ethane tether, is formed on coordination. Crystals of **2** and **6** suitable for X-ray crystallography were obtained on slow evaporation of aqueous solutions of the complexes. The crystal structures of $[Ni(tacn)_2](NO_3)Cl\cdot H_2O$,[12] **3**,[9] **4**[10] and **5**[10] have been described previously.

Crystal structures

The structure of **2** consists of discrete mononuclear $[NiL^{eth}]^{2+}$ cations (Fig. 2, Table 1) and perchlorate anions. The nickel(II) centre is coordinated facially by the two tacn rings of L^{eth}, forming an *intra*molecular sandwich structure. The cation possesses a C_2 axis of symmetry passing through the nickel(II) centre and the middle of the C–C bond of the ethane linker. The geometry about the nickel(II) centre is distorted from regular octahedral. This is due in part to the constraints imposed by the three edge-sharing, five-membered chelate rings of the tacn moieties, which result in acute intra-ring N–Ni–N "bite" angles involving *cis*-disposed N atoms [81.48(7)–83.29(7)°]. Similar values were

Table 1 Selected bond distances (Å) and angles (°) for **2**

Ni–N(1)	2.123(2)	Ni–N(2)	2.105(2)
Ni–N(3)	2.138(2)		
N(1)–Ni–N(1)*	84.37(9)	N(1)–Ni–N(2)	83.29(7)
N(1)–Ni–N(2)*	161.33(7)	N(1)–Ni–N(3)	81.48(7)
N(1)–Ni–N(3)*	109.72(7)	N(2)–Ni–N(2)*	111.8(1)
N(2)–Ni–N(3)	82.20(7)	N(2)–Ni–N(3)*	89.57(7)
N(3)–Ni–N(3)*	165.3(1)		

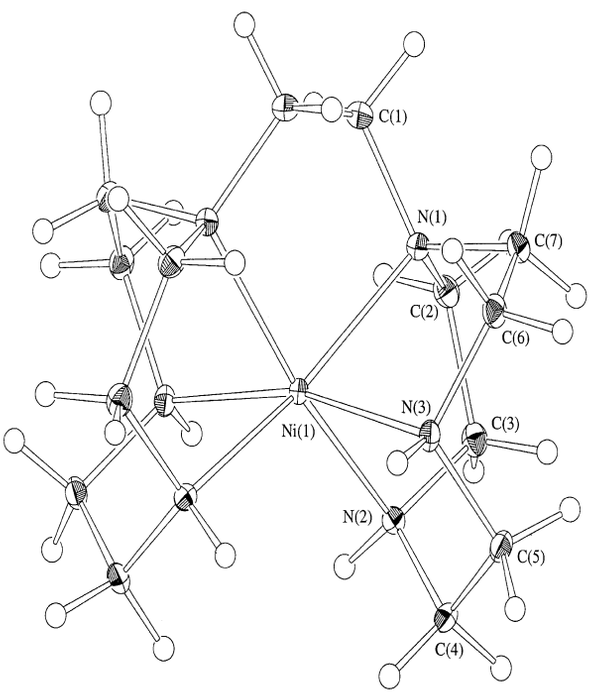

Fig. 2 ORTEP plot of the molecular cation in **2** with thermal ellipsoids drawn at the 30% probability level.

observed for $[Ni(tacn)_2](NO_3)Cl{\cdot}H_2O$ [82.2(6)–83.1(6)°],[13] as well as other nickel(II) complexes of tacn-derived ligands (Table 3). In addition to this trigonal distortion, however, the ethane tether results in further distortion. This is most obvious from the N(1)–Ni–N(1)* angle subtending the ethane linker [84.37(9)°], which is considerably smaller than the inter-ring *cis* N–Cu–N angles observed in $[Ni(tacn)_2](NO_3)Cl{\cdot}H_2O$, and the *trans* N–Ni–N angles [161.33(7)–165.3(1)°], which are also smaller than those found in the latter (see Table 3). Moreover, there is considerable variation in the inter-ring N–Cu–N bite angles [84.37(9)–111.8(1)°] and the Ni–N bond lengths [2.105(2)–2.138(2) Å] in **2**. In comparison, the Ni–N bond lengths in $[Ni(tacn)_2](NO_3)Cl{\cdot}H_2O$ are close to the optimum value of 2.08 Å for octahedral NiN_6 systems (Table 3), and reflect the more symmetric coordination environment provided by the unsubstituted tacn macrocycle.[14] In addition to the steric constraints imposed by the ethane linker, the introduction of less strongly coordinating tertiary amine nitrogens may be responsible for the greater variation and lengthening of the Ni–N bonds in **2** relative to those in $[Ni(tacn)_2](NO_3)Cl{\cdot}H_2O$. This is supported by the presence of a *trans* influence in **2**, *viz*. the Ni–N (*sec* amine) distances *trans* to the bridgehead N′s are shorter [Ni–N(2) 2.105(2) Å] than those for the pair of *trans* secondary amines [Ni–N(3) 2.138(2) Å].

The crystal structure of **6** consists of discrete binuclear $[Ni_2L^{isomes}(H_2O)_3]^{4+}$ cations (Fig. 3, Table 2), perchlorate anions and waters of crystallisation. The analysis confirms the hybrid nature of the compound, with L^{isomes} adopting two distinct modes of coordination towards nickel(II). One Ni(II) centre is sandwiched by a pair of *ortho*-oriented tacn rings while the other Ni(II) is bound to a single tacn unit; its coordination sphere is completed by three water ligands. This mono-tacn coordinated Ni(II) centre lies on the opposite side of the plane of the benzene ring relative to Ni(1), most likely due to a combination of electrostatic and steric effects, resulting in a large Ni · · · Ni separation of 7.87 Å.

Table 2 Selected bond distances (Å) and angles (°) for **6**

Ni(1)–N(1)	2.118(6)	Ni(1)–N(2)	2.099(6)
Ni(1)–N(3)	2.134(6)	Ni(1)–N(4)	2.174(7)
Ni(1)–N(5)	2.128(6)	Ni(1)–N(6)	2.103(6)
Ni(2)–O(1)	2.054(7)	Ni(2)–O(2)	2.083(5)
Ni(2)–O(3)	2.119(6)	Ni(2)–N(7)	2.138(6)
Ni(2)–N(8)	2.050(7)	Ni(2)–N(9)	2.099(7)
N(1)–Ni(1)–N(2)	81.2(2)	N(1)–Ni(1)–N(3)	82.2(2)
N(1)–Ni(1)–N(4)	102.4(2)	N(1)–Ni(1)–N(5)	103.3(2)
N(1)–Ni(1)–N(6)	173.7(2)	N(2)–Ni(1)–N(3)	81.5(3)
N(2)–Ni(1)–N(4)	171.2(3)	N(2)–Ni(1)–N(5)	89.7(3)
N(2)–Ni(1)–N(6)	96.6(3)	N(3)–Ni(1)–N(4)	106.9(3)
N(3)–Ni(1)–N(5)	168.8(2)	N(3)–Ni(1)–N(6)	91.6(2)
N(4)–Ni(1)–N(5)	81.7(3)	N(4)–Ni(1)–N(6)	80.7(2)
N(5)–Ni(1)–N(6)	82.6(2)	O(1)–Ni(2)–O(2)	90.1(3)
O(1)–Ni(2)–O(3)	86.4(3)	O(1)–Ni(2)–N(7)	94.3(3)
O(1)–Ni(2)–N(8)	178.0(3)	O(1)–Ni(2)–N(9)	96.1(3)
O(2)–Ni(2)–O(3)	89.0(2)	O(2)–Ni(2)–N(7)	96.4(2)
O(2)–Ni(2)–N(8)	91.5(2)	O(2)–Ni(2)–N(9)	173.7(3)
O(3)–Ni(2)–N(7)	174.5(2)	O(3)–Ni(2)–N(8)	94.8(3)
O(3)–Ni(2)–N(9)	90.1(3)	N(7)–Ni(2)–N(8)	84.3(2)
N(7)–Ni(2)–N(9)	84.4(3)	N(8)–Ni(2)–N(9)	82.3(3)

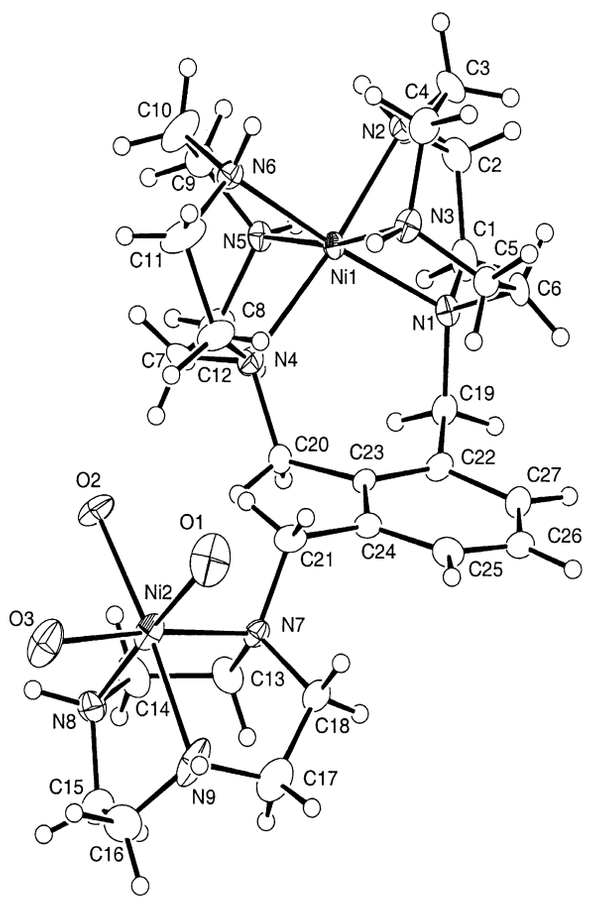

Fig. 3 ORTEP plot of the molecular cation in **6** with thermal ellipsoids drawn at the 30% probability level.

Not surprisingly, the coordination geometry of the sandwiched Ni(1) centre in **6** is very similar to that of the sandwiched nickel(II) centres in **3**,[9] **4**[10] and **5**,[11] in which the metal centres are also bound by *ortho* oriented tacn moieties (Table 3). Thus, the Ni–N bond lengths [2.099(7)–2.174(7) Å] show

Table 3 Selected structural parameters for sandwiched Ni^{II} centres in nickel(II) complexes

Complex	Ni–N distances/Å	Intra-ring N–Ni–N bite angles (°)	N–Ni–N bridgehead angle (°)	Inter-ring N–Ni–N bite angles (°)	Inter-ring *trans*-N–Ni–N angles (°)
$[Ni(tacn)_2](NO_3)Cl\cdot H_2O$ [a]	2.093(4)–2.116(4)	82.2(6)–83.1(6)	—	95.1(6)–99.9(6)	176.0(6)–177.2(6)
2	2.105(2)–2.138(2)	81.5(1)–83.3(1)	84.4(1)	84.4(1)–111.8(1)	161.3(1)–165.3(1)
3 [b]	2.110(4)–2.182(4)	79.3(1)–82.4(1)	103.6(1)	90.5(1)–105.3(1)	169.7(1)–173.9(1)
4 [c]	2.086(4)–2.193(6)	80.0(2)–82.6(2)	103.1(2)	90.3(3)–106.6(3)	169.2(2)–173.4(3)
5 [c]	1.99(3)–2.21(3)	78(1)–83(1)	102(1)	88(1)–108(1)	167(1)–174.1(9)
6	2.099(7)–2.174(7)	80.7(2)–82.6(2)	102.4(2)	89.7(3)–106.9(3)	168.8(2)–173.7(2)
$[Ni(Bztacn)_2][PF_6]_2$ [d]	2.089(4)–2.262(4)	80.3(2)–81.8 (2)	—	90.2(2)–109.0(1)	170.3(2)–178.8(2)

[a] Ref. 13. [b] Ref. 9. [c] Ref. 10. [d] Ref. 15.

Table 4 Electronic spectra of nickel(II) complexes of ligands derived from 1,4,7-triazacyclononane measured in CH_3CN

Complex	λ_{max}/nm (ε_{max}/M^{-1} cm^{-1})
1	327 (5), 506 (5), 560 (sh), 800 (7), 880 (sh)
2	366 (15), 522 (16), 849 (31), 924 (32)
3	347 (10), 359 (10), 538 (8), 625 (sh), 840 (sh), 917 (17)
4	347 (19), 360 (19), 536 (13), 625 (sh), 840 (sh), 917 (29)
5	335 (sh), 535 (29), 830 (sh), 885 (58)
6	340 (19), 534 (17), 830 (sh), 884 (35)
$[Ni(Bztacn)_2][PF_6]_2$ [a]	390 (18), 532 (6), 840 (sh), 961 (11)

[a] Ref. 15.

considerably more variation than observed within the structure of $[Ni(tacn)_2](NO_3)Cl\cdot H_2O$,[12] and the inter-ring *cis* N–Ni–N angles involving either one or both of the bridgehead nitrogens [102.4(2)–106.9(3)°] are enlarged relative to those involving pairs of secondary nitrogens [89.7(3)–96.6(3)°]. This indicates that the aromatic spacer prevents the sandwiching macrocycles from approaching the nickel(II) centre as closely as in $[Ni(tacn)_2](NO_3)Cl\cdot H_2O$. Further evidence for the molecular strain induced in the cation by the aromatic spacer is provided by the fact that the longest Ni–N bond [2.174(7) Å] is associated with one of the tertiary bridgehead nitrogens, N(4), and the considerably enlarged N(4)–C(20)–C(23) angle [118.5(6)°]. The intra-ring *cis* N–Ni–N angles [80.7(2)–82.6(2)°] and *trans* N–Ni–N angles [168.8(2)–173.7(2)°] are again reduced significantly from those expected for an undistorted octahedron.

The distorted octahedral geometry of the mono tacn-coordinated Ni(2) centre in **6** parallels that observed in $[Ni_2L^{px}(H_2O)_6](ClO_4)_4\cdot 3H_2O$ [L^{px} = 1,4-bis(1,4,7-triazacyclonon-1-ylmethyl)benzene][9] and **5**.[10] Notably, the longest Ni(2)–N bond is associated with the tertiary bridgehead nitrogen, N(7) [2.138(6) Å]. The intra-ring N–Ni–N bite angles [82.3(3)–84.4(4)°] are below 90°, whilst the *trans* N–Ni–O angles [173.7(3)–178.0(3)°] are on average closer to the ideal 180° than the *trans* N–Ni–N angles observed for the sandwiched Ni(1) centre. This is to be expected since the NiN_3O_3 coordination sphere is free of the steric constraints that are introduced by sandwiching a nickel centre between two linked tacn macrocycles.

Electronic spectra

Electronic spectral data for the nickel(II) recorded in acetonitrile are summarised in Table 4 together with that of the related nickel complex, $[Ni(Bztacn)_2][PF_6]_2$ (where Bztacn = 1-benzyl-1,4,7-triazacyclononane).[15] The data for **1** and **2** are in excellent agreement with literature data for aqueous solutions of the complexes.[5,16] Each complex shows three maxima typical of octahedral nickel(II) complexes which arise predominantly from spin-allowed $^3A_{2g} \rightarrow {}^3T_{2g}$ (1000–800 nm), $^3A_{2g} \rightarrow {}^3T_{1g}(F)$ (550–500 nm) and $^3A_{2g} \rightarrow {}^3T_{1g}(P)$ (300–400 nm) transitions.[17,18] In each case, the low energy band is asymmetric or has a shoulder. This may be attributed to symmetry splitting or spin–orbit splitting of the $^3T_{2g}$ state, or the close approach of the $^1E_{2g}$ state such that the spin forbidden $^3A_{2g} \rightarrow {}^1E_{2g}$ transition gains intensity through spin–orbit coupling with the $^3T_{2g}$ state.[18,19]

If, as is common practice, the wavelength of maximum absorbance in the 800–1000 nm is taken as a measure of the ligand field splitting parameter, $10Dq$, the data for the sandwiched nickel(II) complexes suggest that the ligand field strengths follow the order tacn ($10Dq$ = 12500 cm^{-1}) > L^{ox} = L^{dur} (10900 cm^{-1} ≈ L^{eth} (10820 cm^{-1}) > Bztacn (10400 cm^{-1}). The weaker ligand fields of L^{eth}, L^{ox}, L^{dur} and Bztacn relative to tacn can be attributed to steric constraints as well as the conversion of one amine in each tacn ring into a tertiary amine. Both of these factors combine to reduce the binding ability of the ligands, as is evident from the Ni–N distances (Table 3). The estimated $10Dq$ values for **5** and **6** of 11300 cm^{-1} indicate a somewhat greater average ligand field strength compared with **2**–**4** and $[Ni(Bztacn)_2][PF_6]_2$.

Hancock and co-workers[18] have cautioned that because of the mixing of $^3T_{2g}$ and $^1E_{2g}$ states, the two bands in the 800–1000 nm region cannot be assigned to pure $^3A_{2g} \rightarrow {}^3T_{2g}$ and $^3A_{2g} \rightarrow {}^1E_{2g}$ transitions. These workers have shown that an empirical relationship, $10Dq = 10630 + 1370\varepsilon_1/\varepsilon_2$ exists between $10Dq$ and the ratio of the coefficients of the uncorrected $^3A_{2g} \rightarrow {}^1E_{2g}$ and $^3A_{2g} \rightarrow {}^3T_{2g}$ transitions ($\varepsilon_1/\varepsilon_2$) which can be used to generate more rational values of $10Dq$. Thus, whilst the bands in the 800–1000 nm region for **2** are in similar positions to those of **3** and **4**, their relative intensities are different, indicating a difference in ligand field strength. Application of the relationship of Hancock and co-workers[17] yields corrected $10Dq$ values of 11940 cm^{-1} for **2** and 11820 cm^{-1} for **3** and **4**. Thus, the ligand field strength of L^{eth} is only marginally greater than that of L^{ox} and L^{dur}.

Electrochemistry

Cyclic, square-wave and near steady-state voltammetry were performed upon the nickel(II) complexes, **1**–**6**, in the range −1.2 to +1.2 V *vs.* the ferrocene–ferrocenium couple ($Fc–Fc^+$). Representative square-wave voltammograms for the mononuclear complex, **2**, and the binuclear complex, **4**, are illustrated in Fig. 4, while Table 5 summarises the electrochemical data for each of the compounds.

Table 5 Cyclic, square-wave and near steady-state voltammetric data for oxidation of nickel(II) complexes in acetonitrile (0.1 M Bu_4NClO_4)[a]

	Cyclic[b]					Square-wave[c]			Near steady-state[d]		
	$E_{1/2}$/V	ΔE_p/mV	I_p^{ox}/μA	I_p^{red}/μA	I_p^{ox}/I_p^{red}	E_p/V	$W_{1/2}$[e]/mV	I_p/μA	I_d[f]/nA	$10^6 D$[g]/cm^2 s^{-1}	n[h]
Fc	0.00	62	4.15	4.15	1.00	0.00	104	13.0	4.77	23	1
1	+0.56	62	2.35	2.41	0.98	+0.56	103	8.6	2.18	10.5	1
2	+0.67	58	2.46	2.49	0.99	+0.67	108	8.7	2.19	10.6	1
3	+0.87	62	2.74	2.71	1.01	+0.86	104	8.6	2.19	10.6	1
4	+0.86	80	3.63	3.57	1.02	+0.87	133	12.1	1.82	4.3	2
5	+0.87	54	1.88	1.85	1.02	+0.86	104	7.1	0.97	4.8	1
6	+0.87	58	1.98	1.98	1.00	+0.87	103	7.2	0.91	4.4	1

[a] Potentials are quoted with respect to the Fc–Fc$^+$ couple used as an internal reference. The current data are normalised to 1.0 mM concentration (c) to facilitate comparison of the values. [b] Cyclic voltammetric data were obtained at a scan rate of 100 mV s^{-1}. [c] Square-wave voltammetric data were measured with a period of 30 ms. [d] Steady-state voltammetric data were measured at a scan rate of 10 mV s^{-1}. [e] $W_{1/2}$ is the estimated width of the peak shaped response at half the wave height. [f] Limiting current under near steady-state conditions. [g] Calculated from limiting current data and use of the relation $I_L = 4nFrcD$ where n = number of electrons, F = Faraday constant, r = electrode radius and D = diffusion coefficient. [h] Total number of electrons associated with process on the basis of self-consistent set of n and D values.

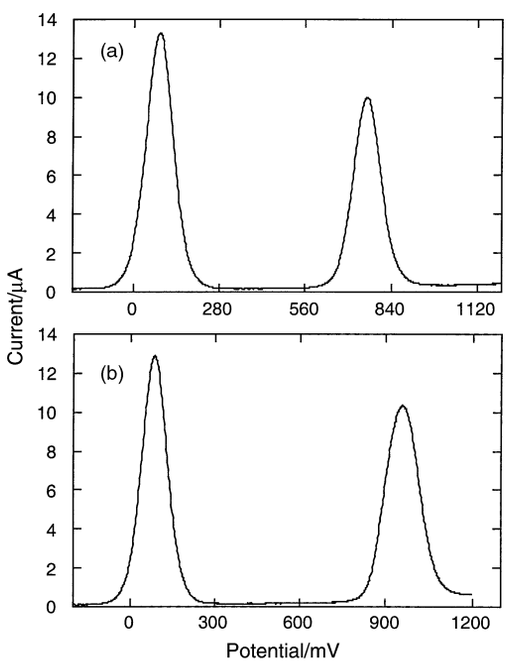

Fig. 4 Square-wave (period = 30 ms) voltammogram of complex **2** (a) and complex **4** (b) recorded in acetonitrile (0.1 M Bu_4NClO_4) using a Pt macrodisk electrode at 20 °C. The initial process is the $Fc^{0/+}$ couple used as internal reference potential standard. The potential axis used is relative to the Ag–Ag$^+$ reference. The broader square-wave voltammogram observed for the binuclear complex **4** is concluded to be composed of two overlapping oxidation–reduction waves, one for each of the Ni(II) centres.

The mononuclear complexes, **1**–**3**, all exhibit redox waves in their cyclic voltammograms corresponding to the reversible oxidation of the sandwiched nickel(II) centres to the nickel(III) state. The chemical reversibility of the observed redox processes is indicated by the ratios of the peak currents accompanying oxidation and reduction (I_p^{ox}/I_p^{red}), which are all close to unity. This is further supported by the fact that the form of the voltammograms did not change on repeated cycling of the potential. The anodic and cathodic peak potential differences (ΔE_p) are close to the theoretical value of 57 mV expected for a fully reversible 1e$^-$ process,[20] and are in agreement with those for the completely reversible $Fc^{0/+}$ process measured under the same conditions. The data are consistent with the presence of only one sandwiched nickel centre within the structures [eqn. (1)].

$$\text{Ni(II)} \rightarrow \text{Ni(III)} + e^- \quad (1)$$

Compounds **5** and **6** show signals with almost exactly the same form ($\Delta E_p \approx 58$ mV) and position ($E_{1/2} \approx 0.87$ V) as compound **3**, which incorporates a similar aromatic tether between the sandwiching tacn macrocycles. This suggests that these signals correspond to the reversible oxidation of the sandwiched nickel(II) centres within these multinuclear complexes. Near-steady state data obtained under microelectrode conditions enable the diffusion coefficients of all complexes to be calculated (Table 5). As expected, the higher molecular weight compounds, **5** and **6** have significantly smaller diffusion coefficients than compounds **1**–**3**. After allowance for the variation of diffusion coefficients it is clear that all data in Table 5 are consistent with reversible one-electron oxidation processes. Irreversible processes evident at very positive potentials probably correspond to the oxidation of the other non-sandwiched nickel centres.

The cyclic and square-wave voltametric response observed for **4** are somewhat broader ($\Delta E_p = 80$ mV, $W_{1/2} = 133$ mV) than those for the other compounds. After analysis of steady-state data and calculated diffusion coefficients (D, Table 5) it is concluded that the voltammetry of **4** is composed of two overlapping oxidation–reduction waves, one for each of the sandwiched nickel centres [eqns. (2) and (3)].

$$\text{Ni(II)Ni(II)} \rightarrow \text{Ni(III)Ni(II)} + e^- \quad (2)$$

$$\text{Ni(III)Ni(II)} \rightarrow \text{Ni(III)Ni(III)} + e^- \quad (3)$$

Richardson and Taube [20] have derived a working curve which allows the determination of $\Delta E_{1/2} = E_{1/2}(2) - E_{1/2}(1)$ for a two-step electrochemical process from the peak-to-peak separation (ΔE_p) of the cyclic voltammogram. Application of this working curve yields a $\Delta E_{1/2}$ value of *ca.* 50 mV for the processes summarised in eqns. (2) and (3). For two non-interacting metal centres, $\Delta E_{1/2}$ will be equal to 36 mV after allowance is made for the statistical factor, $RT/F \ln 4$.[5,21] Thus, the value obtained for **4** suggests that the two sandwiched nickel(II) centres within the compound have some influence on each other. This can be rationalised on the basis that following oxidation of the first nickel centre, the second nickel centre becomes more difficult to oxidise because of the higher charge on the adjacent oxidised centre, and hence the two redox processes, [eqns. (2) and (3)], occur at slightly different potentials. This behaviour has also been observed for the binuclear nickel(II) complexes of a series of bis(pentadentate) ligands derived from bis(tacn) macrocycles.[22] Despite this, similar $E_{1/2}$ values are observed for the sandwich complexes, **3**–**6**.

The nickel(II)/(III) couples for **2**–**6** are all shifted to more positive potentials relative to the $[Ni(tacn)_2]^{2+/3+}$ couple, indicating substantial destabilisation of the nickel(III) state. This is

postulated to be a consequence of the additional strain induced in the bridged ligands upon accommodating the requirements of the smaller nickel(III) ion, combined with the substitution of secondary amine nitrogens for tertiary nitrogens, which would be expected to stabilise the reduced state. The finding that complexes **3**–**6** require the most positive potentials for oxidation is not unexpected in view of the X-ray structural data (Table 3). In particular, the large N–Ni–N angles subtending the aromatic bridges in these complexes indicate that the nickel(II) centre is already too small to fit optimally between the sandwiching macrocycles because of the spacer size. An even greater degree of strain would be expected on moving to the nickel(III) state.

Schröder and co-workers[15] have investigated the electrochemistry of the nickel(II) sandwich complex, $[Ni(Bztacn)_2][PF_6]_2$, and also noted a positive shift in the potential of the nickel(II)/(III) couple relative to that of $[Ni(tacn)_2]^{2+/3+}$. The observed shift of 0.21 V, in this case ascribed to the steric bulk of the pendant benzyl groups, is greater than that for the complex of L^{eth}, but is not as pronounced as those observed for the complexes of L^{ox}, L^{dur} and L^{isomes}. Interestingly, however, this oxidation–reduction process[15] was only found to be chemically reversible when the temperature was lowered to 235 K. The unstable nickel(III) species, $[Ni(Bztacn)_2]^{3+}$, was proposed to undergo a decomposition process involving loss of the benzyl groups to generate $[Ni(tacn)_2]^{3+}$. For the complexes of L^{ox}, L^{dur} and L^{isomes}, the linkage of the sandwiching tacn rings appears to enhance the chemical robustness of the nickel(III) species, leading to reversible redox behaviour, even though more positive potentials are required for their generation.

Conclusions

The sandwiched nickel(II) centres in the series of complexes, **1**–**6**, may be reversibly oxidised to the nickel(III) state at a potential that is tuned by the ability of the tether to accommodate the requirements of the smaller nickel(III) ion. The $[Ni(tacn)_2]^{3+}$ complex has been found to be a convenient outer-sphere one-electron oxidant in electrochemical studies because of the absence of any proton-related equilibria.[12,23] The results of this study indicate that the nickel(III) sandwich complexes of L^{eth}, L^{ox}, L^{dur} and L^{isomes} might prove similarly useful as strong oxidants. In particular, the binuclear nickel(III) complex of L^{dur} could be of practical use in synthetic chemistry (*e.g.* oxidation of organic compounds), by virtue of its ability to undergo a two-electron reduction at essentially a single potential.

Experimental

Materials and reagents

Reagent or analytical grade chemicals, obtained from commercial suppliers, were used without further purification. Literature methods were used to prepare $[Ni(tacn)_2](ClO_4)_2$ (**1**),[12] $[NiL^{eth}](ClO_4)_2$ (**2**),[5] $[NiL^{ox}](ClO_4)_2\cdot H_2O$ (**3**),[9] $[Ni_2L^{dur}](ClO_4)_4\cdot 2H_2O$ (**4**)[10] and $[Ni_3L^{dur}(H_2O)_3](ClO_4)_6\cdot 9H_2O$ (**5**).[10]

Physical measurements

^1H and ^{13}C NMR spectra were recorded in $CDCl_3$ on a Bruker AC200 spectrometer and are referenced relative to tetramethylsilane. The electrospray ionization (ESI) mass spectrum of **6** was recorded in a 1:1 CH_3CN–H_2O mixture on a Micromass Platform quadrupole mass spectrometer. The quoted *m*/*z* values correspond to the most intense peak in each signal envelope. Infrared spectra were recorded as KBr pellets on a Perkin-Elmer 1600 FTIR spectrometer and electronic spectra on a Cary 5G UV-Vis-NIR spectrophotometer. Electron microprobe analysis was made with a JEOL JSM-1 scanning electron microscope through an NEC X-ray detector and pulse-processing system connected to a Packard multichannel analyzer. Cyclic, square-wave and steady-state voltammograms were recorded on a Cypress CS 1090 system. All measurements were made under an atmosphere of nitrogen using a three-electrode potentiostatted system in dry, degassed acetonitrile containing *ca.* 1 mM sample and 0.1 M Bu_4NClO_4 as the supporting electrolyte. A Pt macrodisk working electrode ($r = 0.5$ mm), Pt auxiliary electrode and Ag/Ag^+ (10 mM $AgNO_3$) reference electrode were employed to measure cyclic and square-wave voltammograms. Near steady-state voltammograms were measured in a Faraday cage using a Pt microelectrode ($r = 5$ μm), Pt auxiliary electrode and Ag/Ag^+ (10 mM $AgNO_3$) reference electrode at a scan rate of 10 mV s^{-1}. The redox potentials ($E_{1/2}$ values) obtained from cyclic voltammograms were taken as the average of the oxidation (E_p^{ox}) and reduction (E_p^{red}) peak potentials, and are given with respect to the ferrocene–ferrocenium couple ($Fc–Fc^+$), which was used as an internal standard (1 mM).

CAUTION: Although no problems were encountered in this work, transition metal perchlorates are potentially explosive and should be prepared in small quantities and handled with care.

Syntheses

1,2,3-Tri(bromomethyl)benzene. A mixture of 1,2,3-trimethylbenzene (31.6 g, 0.263 mmol) and *N*-bromosuccinimide (150.0 g, 0.843 mmol) in carbon tetrachloride (700 mL) was refluxed overnight whilst being illuminated with a halogen lamp. After cooling to room temperature, the precipitated succinimide, which formed as a crust on the surface of the reaction mixture, was removed by filtration and the volume of the filtrate reduced on a rotary evaporator until a white solid began to form. The mixture was refrigerated overnight and the precipitate collected by filtration. Recrystallisation from a chloroform–light petroleum (bp 60–70° C) ether mixture afforded a white crystalline product (30.7 g, 33%). δ_H(200.13 MHz): 4.62 (4 H, s, CH_2), 4.83 (2 H, s, CH_2), 7.24–7.38 (3 H, m, aromatic CH); δ_C (50.32 MHz): 24.69, 29.85 (CH_2), 129.72, 131.83 (aromatic CH), 135.70, 138.02 (aromatic quaternary C).

1,2,3-Tris(1,4,7-triazacyclonon-1-ylmethyl)benzene (L^{isomes}). A hot solution of 1,2,3-tri(bromomethyl)benzene (0.55 g, 1.54 mmol) in acetonitrile (10 mL) was added to a stirred solution of 1,4,7-triazatricyclo[5.2.1.$0^{4,10}$]decane (0.65 g, 4.67 mmol) in acetonitrile (10 mL), resulting in the almost immediate formation of a white precipitate. After stirring for 3 days, the precipitate was filtered off; washed with acetonitrile (2 × 30 mL) and diethyl ether (2 × 50 mL) and dried in a vacuum desiccator. The solid was then dissolved in water (50 mL) and refluxed for 3 h. Sodium hydroxide pellets (1.50 g, 37.5 mmol) were carefully added in portions to the solution and reflux continued for a further 4.5 h. After cooling to room temperature, the solution was extracted with chloroform (4 × 50 mL), the combined extracts dried over magnesium sulfate, filtered and reduced to dryness on a rotary evaporator. This yielded the crude ligand as a fluffy white solid (0.57 g, 74%), which was used directly in the preparation of the nickel(II) complex. δ_H(200.13 MHz): 3.07 (8 H, t, CH_2), 3.34 (8 H, t, CH_2), 3.48 (4 H, s, CH_2), 3.72 (12 H, m, CH_2), 3.93 (2 H, s, CH_2), 4.28 (4 H, m, CH_2), 5.03 (2 H, s, CH_2), 5.16 (2 H, s, CH_2), 7.42–7.46 (1 H, m, aromatic CH) 7.53–7.56 (2 H, m, aromatic CH); δ_C(50.32 MHz): 42.55, 42.72, 43.24, 44.34, 45.96, 48.60, 56.23, 58.20 (CH_2), 130.24, 131.06 (aromatic CH) 132.51, 132.66 (aromatic quaternary C).

$[Ni_2L^{isomes}(H_2O)_3](ClO_4)_4\cdot 9H_2O$ (6). To an aqueous solution (50 mL) of L^{isomes} (0.25 g, 0.5 mmol) and $Ni(NO_3)_2\cdot 6H_2O$ (0.50 g, 1.72 mmol), heated on a steam bath, a solution of 2 M sodium hydroxide was added dropwise until a small amount of nickel hydroxide precipitate appeared which would not dissolve

Table 6 Crystal data for $[NiL^{eth}](ClO_4)_2$ (**2**) and $[Ni_2L^{isomes}(H_2O)_3](ClO_4)_4 \cdot 7H_2O$ (**6**)

Formula	$C_{14}H_{28}Cl_2N_3NiO_8$	$C_{27}H_{71}Cl_4Ni_2N_9O_{26}$
M/g mol^{-1}	542.05	1197.11
Crystal system	Orthorhombic	Triclinic
Space group	*Pbcn* (no. 60)	$P\bar{1}$(no. 2)
a/Å	14.1402(2)	9.5317(3)
b/Å	9.6023(1)	15.6344(5)
c/Å	16.4655(2)	16.8035(4)
α/°	90	92.521(5)
β/°	90	91.116(2)
γ/°	90	105.705(1)
U/Å^3	2235.66(9)	2407.0(1)
Z	4	2
T/K	123	123
λ/Å	0.71069	0.71069
D_c/ g cm^{-3}	1.610	1.652
μ(Mo–Kα)/ cm^{-1}	11.60	10.99
No. of reflections measured	3679	12062
No. of reflections ($I \geq 3\sigma(I)$)	2518	6366
R^a	0.037	0.092
R'^b	0.042	0.104
ρ_{min},ρ_{max} /e Å^{-3}	−0.46, 1.36	−1.35, 1.39

^{a} $R = \Sigma(||F_o| - |F_c||)/\Sigma|F_o|$. ^{b} $R' = [\Sigma w(|F_o| - |F_c|)^2/\Sigma wF_o^2]^{1/2}$, where $w = [\sigma^2(F_o)]^{-1}$.

on prolonged heating. Sufficient 2 M hydrochloric acid was then added to just dissolve this precipitate and the resulting purple–blue solution heated for a further 15 min before being diluted to 2 L with water and loaded onto a Sephadex SP-C25 column (H^+ form, 15 × 4 cm). After washing the column with water and 0.1 M sodium perchlorate (to remove a green band of excess Ni^{2+}), a purple–pink band was eluted with 0.5 M sodium perchlorate. On standing overnight this fraction yielded purple–pink needles of **6**, which were collected by vacuum filtration, washed with methanol and air-dried (0.27 g, 45%). Microanalyses: $C_{27}H_{71}Cl_4N_9Ni_2O_{26}$ {$[Ni_2L^{isomes}(H_2O)_3](ClO_4)_4 \cdot 7H_2O$} requires C, 27.1; H, 5.9; N, 10.6. Found: C, 26.2; H, 5.1; N, 10.4%. ESI mass spectrum: m/z 916.2 $[Ni_2L^{isomes}(ClO_4)_3]^+$, 408.6 $[Ni_2L^{isomes}(ClO_4)_2]^{2+}$, 239.2 $[Ni_2L^{isomes}(ClO_4)]^{3+}$. Electron microprobe: Ni and Cl present. Selected IR bands (ν_{max}/cm^{-1}): 3421s (br), 3320s, 2937m, 1627m (br), 1492m, 1461m, 1365w, 1145s, 1087s, 628s.

A second, faint purple–blue band, presumed to be $[Ni_3L^{isomes}(H_2O)_9]^{6+}$, was subsequently eluted using 1 M sodium perchlorate but attempts to crystallise this complex were unsuccessful due to its very high solubility.

Crystallography

Intensity data for a pink crystal of **2** (dimensions *ca.* 0.18 × 0.18 × 0.18 mm) and purple–pink crystal of the heptahydrate of **6** (dimensions 0.15 × 0.13 × 0.09 mm) were measured at 123 K on a Nonius Kappa CCD fitted with graphite-monochromated Mo-Kα radiation (0.71069 Å). Data were collected to maximum 2θ values of 60.0 and 60.2° for **2** and **6**, respectively, and processed using the Nonius software.[24] The structures were solved by direct methods and expanded using standard Fourier routines in the TeXsan software package.[25] All non-hydrogen atoms were refined with anisotropic thermal parameters. Hydrogens were included in calculated positions but not refined. Neutral atom scattering factors were those incorporated in the TeXsan program. Refinement was against F [sigma weights, *i.e.*, $1/\sigma^2(F)$]. Crystal parameters and details of the data collection, solution and refinement are summarised in Table 6. The rather high R-value for structure **6** is due to the high thermal motion of perchlorate anions and water molecules. ORTEP [26] perspectives of the complexes are presented in Fig. 2 and 3, and selected bond lengths and angles in Tables 1 and 2.

CCDC reference numbers 159103 and 159104.

See http://www.rsc.org/suppdata/dt/b1/b101766g/ for crystallographic data in CIF or other electronic format.

Acknowledgements

This work was supported by ARC grants to A. M. B., M. T. W. H. and L. S. B. G. was the recipient of an Australian Postgraduate Award.

References

1 H. Koyama and T. Yoshino, *Bull. Chem. Soc. Jpn.*, 1972, **45**, 481.
2 P. Chaudhuri and K. Wieghardt, *Prog. Inorg. Chem.*, 1987, **35**, 329.
3 K. Wieghardt, *Pure Appl. Chem.*, 1988, **60**, 509.
4 N. Tanaka, Y. Kobayashi and S. Takamoto, *Chem. Lett.*, 1977, 107.
5 K. Wieghardt, I. Tolksdorf and W. Herrmann, *Inorg. Chem.*, 1985, **24**, 1230.
6 X. Zhang, W.-Y. Hsieh, T. N. Margulis and L. J. Zompa, *Inorg. Chem.*, 1995, **34**, 2883.
7 R. Haidir, M. Ipek, B. DasGupta, M. Yousaf and L. J. Zompa, *Inorg. Chem.*, 1997, **36**, 3125.
8 B. DasGupta, C. Katz, T. Israel, M. Watson and L. J. Zompa, *Inorg. Chim. Acta*, 1999, **292**, 172.
9 B. Graham, G. D. Fallon, M. T. W. Hearn, D. C. R. Hockless, G. Lazarev and L. Spiccia, *Inorg. Chem.*, 1997, **36**, 6366.
10 B. Graham, M. J. Grannas, C. Kepert, L. Spiccia, M. T. W. Hearn, B. W. Skelton and A. H. White, *Inorg. Chem.*, 2000, **39**, 1092.
11 L. Spiccia, B. Graham, M. T. W. Hearn, G. Lazarev, B. Moubaraki, K. S. Murray and E. R. T. Tiekink, *J. Chem. Soc., Dalton Trans.*, 1997, 4089.
12 A. McAuley, P. R. Norman and O. Olubuyide, *Inorg. Chem.*, 1984, **23**, 1938.
13 L. J. Zompa and T. N. Margulis, *Inorg. Chim. Acta*, 1978, **28**, L157.
14 R. D. Hancock, *Prog. Inorg. Chem.*, 1989, **37**, 187.
15 A. J. Blake, I. A. Fallis, S. Parsons, S. A. Ross and M. Schröder, *J. Chem. Soc., Dalton Trans.*, 1996, 525.
16 K. Wieghardt, W. Schmidt, W. Herrmann and H.-J. Küppers, *Inorg. Chem.*, 1983, **22**, 2953.
17 D. Sutton, *Electronic Spectra of Transition Metal Complexes*, McGraw-Hill, London, 1968.
18 S. M. Hart, J. C. A. Boeyens and R. D. Hancock, *Inorg. Chem.*, 1983, **22**, 982.
19 R. Stranger, S. C. Wallis, L. R. Gahan, C. H. L. Kennard and K. A. Byriel, *J. Chem. Soc., Dalton Trans.*, 1992, 2971.
20 D. E. Richardson and H. Taube, *Inorg. Chem.*, 1981, **20**, 1278.
21 R. R. Gagné and C. L. Spiro, *J. Am. Chem. Soc.*, 1980, **102**, 1443.
22 S. J. Brudenell, P. C. Mahon, L. Spiccia, A. M. Bond and D. C. R. Hockless, *Inorg. Chem.*, 2000, **39**, 881.
23 A. McAuley, L. Spencer and P. R. West, *Can. J. Chem.*, 1985, **63**, 1198.
24 Z. Otwinowski and W. Minor, DENZO-SMN Manual, University of Texas Southwestern Medical Center, Dallas, 1997.
25 teXsan, Crystal Structure Analysis Package, Molecular Structure Corporation, Houston, TX, 1985.
26 C. K. Johnson, ORTEP II, Report ORNL-5138, Oak Ridge National Laboratory, Oak Ridge, TN, 1976.